01 Dec 2018

Synergic Titanium Nitride Coating and Titanium Doping by Atomic Layer Deposition for Stable- and High-Performance $LiFePO_4$

Yan Gao

Jonghyun Park
Missouri University of Science and Technology, parkjonghy@mst.edu

Xinhua Liang
Missouri University of Science and Technology, liangxin@mst.edu

Recommended Citation

Y. Gao et al., "Synergic Titanium Nitride Coating and Titanium Doping by Atomic Layer Deposition for Stable- and High-Performance $LiFePO_4$," *Journal of the Electrochemical Society*, vol. 165, no. 16, ECS, Dec 2018.
The definitive version is available at https://doi.org/10.1149/2.0671816jes

Synergic Titanium Nitride Coating and Titanium Doping by Atomic Layer Deposition for Stable- and High-Performance Li-Ion Battery

Yan Gao,[1] Jonghyun Park,[2,*] and Xinhua Liang[1,*,z]

[1]*Department of Chemical and Biochemical Engineering, Missouri University of Science and Technology, Rolla, Missouri 65409, USA*
[2]*Department of Mechanical & Aerospace Engineering, Missouri University of Science and Technology, Rolla, Missouri 65409, USA*

Atomic layer deposition (ALD) method has emerged as a promising technique to address the dissolution and poor conductivity of electrode materials of lithium ion batteries. In this work, surface modification of $LiFePO_4$ (LFP) was carried out by titanium nitride (TiN) ALD, during which a Ti doping into LFP occurred simultaneously. X-ray photoelectron spectroscopy (XPS) and electrochemical tests were performed to prove the Ti doping, and the composition of TiN layer on the surface of LFP particles was interpreted as a combination of TiN and titanium oxynitride (TiO_xN_y). Owing to the synergy of TiN coating and Ti doping, the specific capacity of the modified LFP particles increased to ~159 mAh/g, compared to ~150 mAh/g of the uncoated one. The modified LFP exhibited a superior cyclic stability with a capacity retention of ~89% after 1,000 cycles of charge-discharge at a 2C rate at room temperature, whereas the failure of uncoated LFP began after only 500 cycles. A significant reduction of impedance was observed on the TiN ALD-modified LFP, and SEM results showed that this modification restricted severe growth of solid permeable interface layer on the surface of cathode.
 [DOI: 10.1149/2.0671816jes]

Manuscript submitted September 24, 2018; revised manuscript received November 8, 2018. Published December 13, 2018.

Lithium ion battery (LIB) cathodes, as one of the limiting factors to the performance of LIB, have been intensively investigated due to cathodes are commonly materials with low conductivity, and they become unstable during long-term cycling, therefore researchers seek effective design and engineering in nanoscale for a higher energy and power density and better stability.[1–3] Atomic layer deposition (ALD), which employs self-limiting vapor-phase reactions, has emerged as a powerful coating technique due to its predominant advantages, such as uniformity of coating and precise control of the coating thickness.[4,5] For LIB cathodes, ALD has been mainly used to provide uniform and protective coating on electrode surface and control thickness of the coating for an optimal performance.[6–11] The use of conductive ALD coating can limit the formation of the passive solid permeable interface (SPI) layer and lower the surface resistance. Recently, a novel approach has been reported to achieve cation doping by post-annealing ALD-coated cathode.[12,13] Adopting ALD for doping will help manipulate the uniformity and adjust amount of dopant cation. The doped phase resided between surface coating and bulk structure of the cathode can alleviate the side reactions between cathode surface and electrolyte, and thus improve the activity of charge transfer reactions.[12]

By combining coating and doping methods, their advantages can be exploited together. To achieve that, one way is to synthesize materials with dopant precursors and perform coating in separate steps. Another way is to perform post-heat-treatment to induce cation diffusion from the coating to the bulk of electrode materials.[12,14] Recently, Liang et al. reported synergic effects of FeO_x coating and Fe doping on a commercial $LiMn_{1.5}Ni_{0.5}O_4$ with one step ALD process, during which Fe diffused from surface to bulk and contributed to the Fe doping.[15] The use of ALD can assure better uniformity of coating and doping than conventional liquid-based methods did, and this way can make use of the high reaction temperature along with ALD for a cation doping.

In this work, we carried out titanium nitride (TiN) ALD on the surface of $LiFePO_4$ (LFP) particles in a fluidized bed reactor. Compared with Al_2O_3 and some other metal oxides, TiN has a higher electronic conductivity and chemical stability, and it also showed good mechanical hardness.[16–19] In the meanwhile, the high reaction temperature of TiN ALD (e.g., 400°C) gave rise to a second reaction between $TiCl_4$ and LFP, which resulted in Ti doping into LFP. By incorporating both surface and bulk modification, the LFP particles modified with 5 cycles of TiN ALD showed a super-stable cyclic performance with a capacity retention of ~89% even after 1,000 cycles of charge-discharge at a 2C (1C = 170 mA/g) rate, as compared to that of uncoated LFP, which was only able to work for about 500 cycles at the same conditions. The results of electrochemical impedance spectroscopy (EIS) exhibited that the modified LFP has a significantly lower surface and charge transfer resistance than that of the uncoated LFP. Through scanning electron microscopy (SEM), we found that the TiN ALD modification strengthened the mechanical stability of LFP and inhibited the severe growth of a SPI layer.

Experimental

ALD film coating.—TiN ALD was applied on commercial LFP particles in a fluidized bed reactor, as described elsewhere.[20] The TiN film was deposited by alternative dose of titanium tetrachloride ($TiCl_4$) (99% pure, Alfa Aesar) and ammonia (NH_3) (99.9%, Airgas) at 400°C, and every dose was followed by a N_2 flush to eliminate unreacted precursors. $TiCl_4$ was evaporated and delivered into a reactor chamber at room temperature with N_2 as a carrier gas. Pristine LFP particles were named as UC, as comparison to modified samples, and LFP particles modified with 5 and 10 cycles of TiN ALD were named as 5c-TiN and 10c-TiN, respectively. For comparison, Al_2O_3 films were also coated on LFP particles, since Al_2O_3 is one of the most commonly used ALD films in the surface modification for LIB electrodes and Al_2O_3 ALD films have been reported to improve the electrochemical performance of LIB electrode materials, though Al_2O_3 is a well-known insulating material. Al_2O_3 ALD was carried out using trimethylaluminum (97%, Sigma-Aldrich) and deionized water as precursors at 177°C. The LFP particles coated with 2, 5, and 10 cycles of Al_2O_3 ALD were named as 2c-Al_2O_3, 5c-Al_2O_3, and 10c-Al_2O_3. All the feed lines were maintained at 120°C to avoid condensation of precursors. To study the mechanism of Ti doping, an experiment of Ti doping was also carried out following the TiN ALD process, but only the half cycle of $TiCl_4$ dose and N_2 flush was

*Electrochemical Society Member.
zE-mail: liangxin@mst.edu

included. In another experiment, at the same condition, N_2 gas and O_2 gas were used to take place of $TiCl_4$ vapor to investigate the possible oxidization of LFP in different atmospheres.

Materials characterization.—The carbon content contained in the uncoated $LiFePO_4$ (UC) cathode particles was examined using a thermogravimetric analysis (TGA). The TGA was carried out using a Q50 thermogravimetric-differential scanning calorimetry (TGA/DSC) (TA instruments) under flowing nitrogen or oxygen gas at atmospheric pressure (40 mL/min) at a heating rate of 20°C/min until 1,000°C. Morphology of the UC powders was observed using a Hitachi S-4700 field emission scanning electron microscope (FE-SEM) equipped with an energy dispersive spectroscopy (EDS) system. The mass percentages of Ti element on TiN ALD modified LFP particles were quantified by inductively coupled plasma atomic emission spectrometer (ICP-AES). The surface area of pristine LFP particles was calculated using the Brunauer–Emmett–Teller (BET) method in a relative pressure range of 0.05–0.25 based on nitrogen adsorption and desorption isotherms obtained by a Quantachrome Autosorb-1. The chemical state of TiN and Al_2O_3 ALD films was verified by X-ray photoelectron spectroscopy (XPS) (Kratos Axis 165) through an introduction of Al Kα radiation, operated at 150 W and 15 kV. The XPS spectra were plotted and analyzed using CASA-XPS software program. The powder X-ray diffraction (XRD) of pristine and modified particles was performed with PANalytical X'Pert Pro multi-purpose diffractometer using CuKα radiation ($\lambda = 1.5406$ Å) and a scan rate of 3°/min.

Coin cell assembly.—A cathode electrode was prepared with slurry using 10 wt% of polymer binder poly(vinylidene fluoride) (PVDF, Alfa Aesar) completely dissolved in N-methyl-2-pyrrolidone (NMP, Sigma-Aldrich) solvent, which was incorporated into a mixture of 80 wt% of uncoated or ALD-modified LFP cathode powders and 10 wt% carbon black (super P conductive, 99+ %, Alfa Aesar). This slurry was then cast on an aluminum foil uniformly using a doctor blade and dried at 120°C for 12 hours in a vacuum oven. The cathode paste was punched into round discs with an area of ~0.71 cm^2. The mass loading of every cathode disc was ~3.5 mg/cm^2. Each disc was cold-pressed with 2.5 metric tons before assembly. CR2032 coin cells were assembled with cathode discs and lithium metal discs (99.99%, Sigma-Aldrich) in an argon-filled glove box. The two electrodes were separated by a Celgard-2320 separator. The electrolyte was lithium hexafluorophosphate ($LiPF_6$, 1 mol/L, Sigma-Aldrich) solution with a solvent of ethylene carbonate (EC) and dimethyl carbonate (DMC) (1:1 volume ratio).

Electrochemical testing.—Galvanostatic charge-discharge cycling tests of coin cells were performed between 2.5 V and 4.2 V by Neware Corporation's battery analyzer. The cyclic voltammetry (CV) was carried out at a scan rate of 0.1 mV/s between 2.5 V and 4.5 V using SP-150 Potentiostat, Bio-Logic Science Instruments SAS. A three-electrode configuration was utilized with lithium metal as both anode and reference electrode. The EIS was performed using the SP-150 Potentiostat, which was the same instrument used for the CV test, in a frequency ranging from 10 mHz to 1 MHz and with an excitation signal of 5 mV at room temperature. The collected EIS data were analyzed with an equivalent circuit model using an EC-Lab software. After 1,000 charge-discharge cycles at a 2C rate, the coin cells of UC and 5c-TiN were disassembled in a glove box under Ar atmosphere to extract the cycled cathode discs; the discs were rinsed and flushed with DMC and then dried under vacuum to remove the residual electrolyte.[21] The acquired cathode discs were visualized using SEM measurements to investigate the morphology change after 1,000 cycles of charge-discharge test.

Results and Discussion

Material characterization.—Pristine LFP particles (Figure S1) exhibited irregular shapes with diameters in a range of 1 to 5 μm. TGA measurements of pristine LFP particles were carried out in N_2 and O_2 atmosphere between room temperature and 1,000°C, as shown in Figure S2. In Figure S2a, water desorption caused a little weight loss, but the flat curve indicated that the LFP kept stable until 400°C in a N_2 atmosphere; however, a weight increase was found beginning from ~350°C in an atmosphere of O_2 (Figure S2b). The weight increase in an O_2 atmosphere indicated the oxidization of LFP particles, which caused the formation of a secondary phase, $Li_3Fe_2(PO_4)_3$.[22] These results also indicated that the LFP particles could be unstable at high temperature in an atmosphere of reactive gas, such as $TiCl_4$ vapor during the TiN ALD process. Besides, according to the TGA results in O_2 atmosphere, a trace amount of carbon was found to exist which was considered of no significant influence on LFP as reported.[23]

The pristine LFP particles were coated with different thicknesses of TiN films by ALD. The mass loading of Ti element in the 5c-TiN and 10c-TiN particles was measured by ICP-AES, which was ~1.03 wt% and ~1.75 wt%, respectively. The surface area of pristine LFP particles was 15 m^2/g based on the BET method. Assume that no diffusion of Ti into LFP occurred and all TiN film covered on the surface of LFP particles, we should be able to calculate the thickness of TiN film based on the Ti content and the surface area of the particles. According to the following equation,

$$\delta = \frac{V_{TiN}}{A} = \frac{\frac{M_{TiN}}{M_{Ti}} \times \omega_{Ti}}{A \times \rho_{TiN}} \quad [1]$$

where δ is the thickness, V is the volume of TiN film, A is the surface area measured by the BET method, M is the molar mass of TiN or Ti, ω is the weight percentage measured by ICP-AES, and ρ is the density of TiN. Therefore, the thicknesses δ was calculated as ~0.17 nm and ~0.29 nm for 5c-TiN and 10c-TiN, respectively, which were too thin to be observed using regular transmission electron microscopes. The film growth rate of TiN was estimated to be ~0.03 nm per cycle, which was comparable to the reported values.[24,25]

The LFP particles were also coated with different thicknesses of Al_2O_3 films by ALD. To investigate the composition of TiN and Al_2O_3, XPS was performed on the UC, 5c-TiN, and 5c-Al_2O_3 samples. In Figure S3, the XPS survey spectrum of UC included all the typical peaks of LFP.[26] In contrast, the XPS survey spectra of the 5c-TiN (Figure S4a) and the 5c-Al_2O_3 (Figure S4b) exhibited Ti 2p and N 1s peaks or Al peaks associated with TiN or Al_2O_3 coating, respectively. The core levels of Ti 2p and N 1s were analyzed by high-resolution XPS measurement for a detailed investigation. In Figure 1a, the N 1s spectrum was deconvoluted into three peaks at binding energies of 395.7 eV, 397.2 eV, and 399 eV. The peak located at 395.7 eV was assigned to nitrogen in the TiO_xN_y or O-Ti-N bond due to the easy oxidization of TiN surface in air after ALD; the peaks at 397.2 eV indicated the existence of Ti^{3+} and Ti-N chemical bond in a stoichiometric TiN; the peak located at 399 eV was attributed to chemisorbed molecular nitrogen.[27,28] In Figure 1b, the doublet peaks of Ti 2p spectrum were corresponding to Ti $2p_{3/2}$ (456.6 eV) and Ti $2p_{1/2}$ (462.5 eV). Deconvolution of Ti $2p_{3/2}$ showed a peak located at 455.3 eV, indicating the Ti^{3+} state in TiN; the peak located at 456.5 eV was related to TiO_xN_y.[27] A peak located at 458 eV evidenced a state of Ti^{4+}, however, this was lower than the binding energy of stoichiometric bonded $TiCl_4$ or TiO_2.[29] The separated Ti $2p_{1/2}$ encompassed a set of peaks at 460.8 eV for TiN, 462.3 eV for TiO_xN_y, and 464 eV for Ti^{4+}.[29] The TiN coating was found to be a combination of TiN and TiO_xN_y, and the presence of Ti^{4+} should be due to the Ti^{4+} from $TiCl_4$ diffused into LFP directly without reacting with NH_3.

To investigate the structure changes of LFP after ALD coating, powder XRD was performed on the pristine, 5c-TiN, and 5c-Al_2O_3 samples. In Figure 2, the labeled peaks were identified as the typical orthorhombic $LiFePO_4$ olivine-type phase (JCPDS No. 40–1499). The peaks of UC and 5c-Al_2O_3 samples showed no obvious difference, since the Al_2O_3 ALD film was amorphous or the Al_2O_3 loading (<1 nm thick) was not enough to be detected by XRD.[15] The 5c-TiN also exhibited those featured peaks of LFP, but some new peaks appeared additionally. These new peaks were interpreted to be $FePO_4$ or the partially delithiated LFP.[30–32] The loss of Li element should be

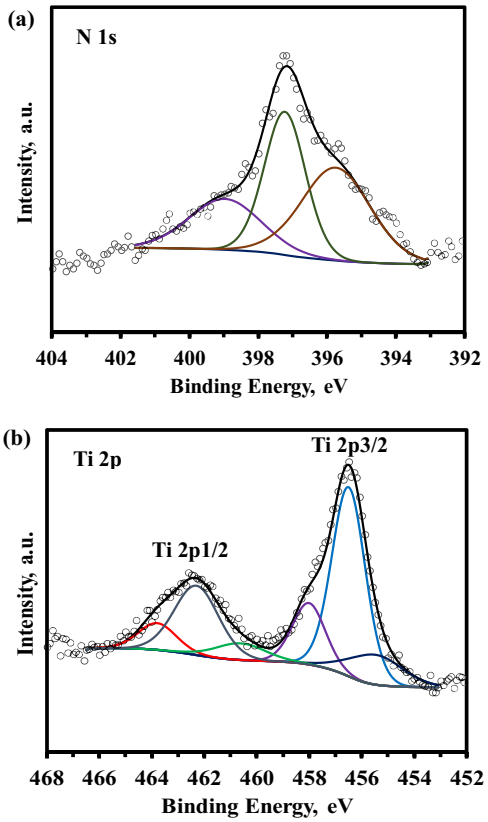

Figure 1. XPS results of (a) N 1s core levels, and (b) Ti 2p core levels of 5c-TiN.

related to the TiN ALD process. The delithiated $LiFePO_4$, i.e., $FePO_4$ phase, was still electrochemically active and was able to be lithiated again during charge-discharge cycling. The vacant site left by delithiation may provide a path for the diffusion of Ti^{4+} into LFP. The Ti^{4+} observed in XPS spectra should be attributed to the diffusion of Ti^{4+} into Li^+ vacancy or occupation of Ti^{4+} on the original deficiency in LFP, without staying on the surface of LFP to react with NH_3 later. In other words, Ti can be doped on LFP particles during the TiN ALD process. No peak related to Ti-included phase was detected by XRD due to its limited amount in the XRD pattern of TiN-coated LFP or amorphous TiN.

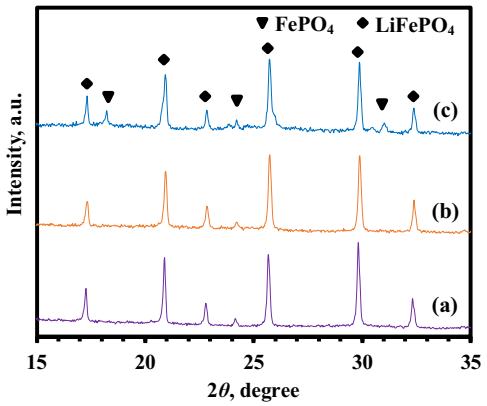

Figure 2. XRD patterns of (a) UC, (b) 5c-Al_2O_3, and (c) 5c-TiN. Diffraction peaks are labeled for orthorhombic structure of LFP with olivine-type phase (diamond) and $FePO_4$ phase (triangle).

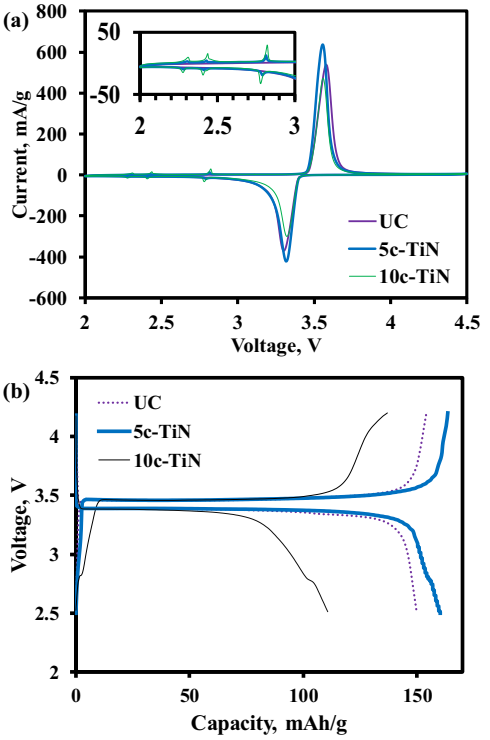

Figure 3. (a) CV results of UC, 5c-TiN, and 10c-TiN at a scan rate of 0.1 mV/s between 2 V and 4.5 V, and (b) the voltage profiles of UC, 5c-TiN, and 10c-TiN at a 0.1C rate between 2.5 V and 4.2 V. The inset figure in (a) is a magnified image between 2 V and 3 V in CV.

Investigation on Ti-doping.—Cyclic voltammetry (CV) of UC, 5c-TiN, and 10c-TiN was performed to investigate the kinetic of the electrochemical reactions. In Figure 3a, the peaks at 3.45 V were observed for all of the three samples, indicating that the main electrochemical reaction was from Fe^{3+}/Fe^{2+} redox couple (Fe peaks). However, after TiN ALD, 5c-TiN and 10c-TiN both exhibited three pairs of reversible peaks (Ti peaks) at ~2.29, ~2.42, and ~2.80 V in addition to 3.45 V. These peaks were attributed to an electrochemical reaction of Ti^{4+}/Ti^{3+} redox couple.[33–35] The ratio of Ti peaks to Fe peaks showed a higher value of ~0.065 for the samples of 10c-TiN (calculated from current intensity of cathodic peak of Ti at ~2.82 V to Fe at ~3.56 V) than ~0.019 of 5c-TiN (Ti at ~2.81 V to Fe at ~3.54 V), which suggested that increasing the cycle numbers of TiN ALD could result in more Ti doping. However, 10c-TiN showed suppressed current intensities of Fe peaks, and this should be due to the fact that the excessive amount of Ti impeded the diffusion of Li^+. In contrast, the enhanced current densities of Fe peaks of 5c-TiN indicated that proper amount of Ti doping could help increase the electrochemical reaction rate. The Fe peak separation of UC, 5c-TiN, and 10c-TiN were ~0.29, ~0.22, and ~0.24 V, respectively, indicating a reduced polarization of the cell due to TiN ALD. In Figure 3b, 5c-TiN delivered a specific capacity of ~159 mAh/g, which is ~93% of theoretical capacity (170 mAh/g of LFP), while 10c-TiN only has a specific capacity of ~110 mAh/g. At ~2.8 V, the plateaus in the voltage profiles of 5c-TiN and 10c-TiN agreed with the CV results, and 10c-TiN showed a longer plateau than that of 5c-TiN at ~2.8 V, which was also consistent with its higher current response at that potential in the CV curve.

The mechanism of Ti doping was investigated by placing the pristine LFP particles in an atmosphere of $TiCl_4$ vapor and heating particles to 400°C. The voltage profiles of these samples are shown in Figure 4. As shown in Figure 4b, three pairs of peaks appeared at 2.84/2.76 V, 2.45/2.38 V, and 2.33/2.25 V, which are rightly consistent with the CV results. There was no reaction between $TiCl_4$ and

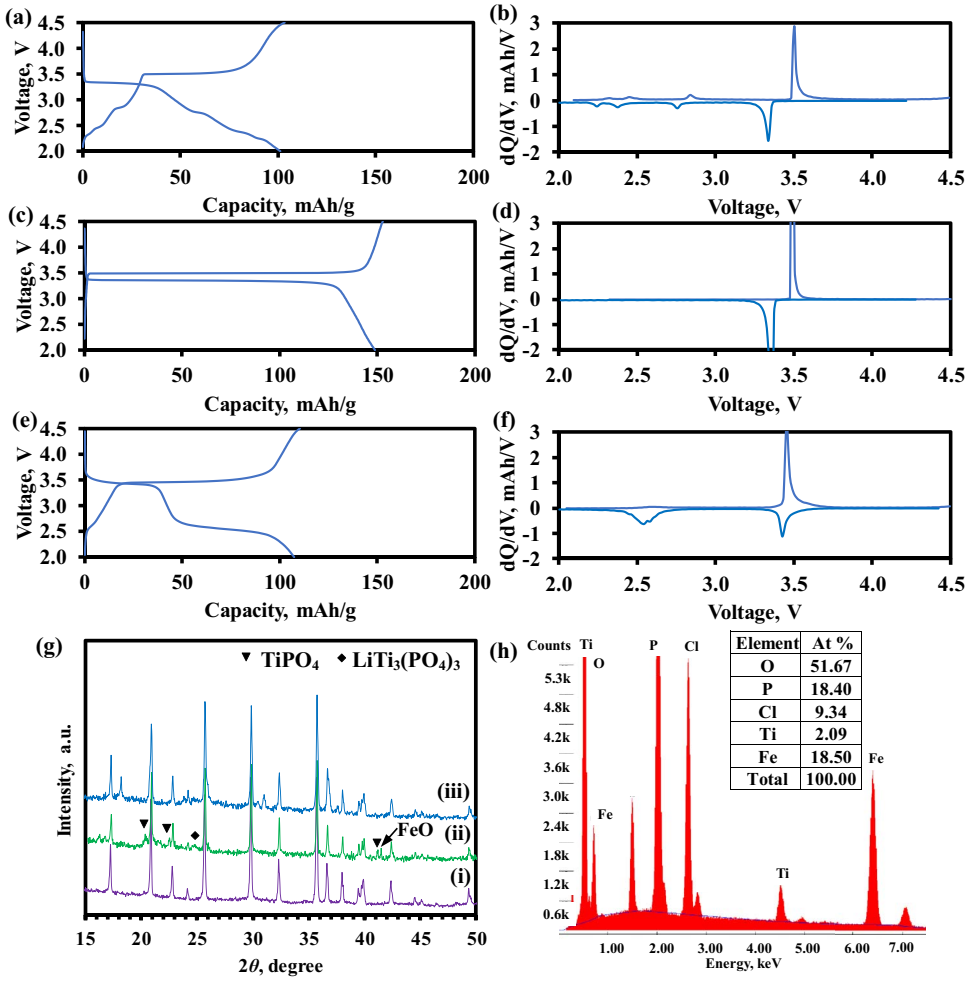

Figure 4. Voltage profiles (a,c,e) and corresponding dQ/dV profiles (b,d,f) of LFP heated at 400°C in an atmosphere of (a,b) $TiCl_4$, (c,d) N_2, and (e,f) O_2; (g) XRD patterns of (i) UC, (ii) $TiCl_4$-modified, and (iii) TiN-coated LFP; and (h) EDS spectrum of $TiCl_4$-modified LFP.

NH_3, so the reaction between $TiCl_4$ and LFP and excessive $TiCl_4$ caused the flat plateau of Fe^{3+}/Fe^{2+} redox couple to be shortened a lot. Koenig et al.[33] and Wang et al.[35] reported that the Ti-doped LFP contained $LiTi_2(PO_4)_3$, which has a lower theoretical capacity than that of pure LFP but a higher electronic conductivity and ionic conductivity for Li^+. A long-time staying in an atmosphere of $TiCl_4$ at high temperature may also cause the charge transfer between Ti^{4+} and Fe^{2+} and thus form Ti^{3+} and Fe^{3+}, or even loss of electrochemically active LFP phase, therefore exposure of LFP to $TiCl_4$ during TiN ALD process should be controlled properly. In an atmosphere of N_2, the pristine LFP particles was also heated to 400°C, but only Fe peaks were found in Figure 4d, which means that the LFP was stable in the flush gas during the ALD process at 400°C. To verify that three pairs of new peaks were not resulted from the oxidization of LFP, the same experiment was performed using O_2 atmosphere. In Figure 4f, the discharge curve showed separated peaks at ∼2.52 V and ∼3.40 V, which should be due to the formation of a secondary phase, $Li_3Fe_2(PO_4)_3$, but different from the Ti-doped LFP. Figure 4g shows the XRD patterns of UC, $TiCl_4$-modified, and TiN-coated LFP particles. No peak of $FePO_4$ was observed after LFP reacted with $TiCl_4$, compared with that of 5c-TiN, but some new peaks appeared which were indexed to Ti-included phosphate. Ti tended to segregate into a Ti-enriched phase, but not to form a solid solution with LFP,[33] so the peak at ∼24.5° in $TiCl_4$-modified LFP ((ii) in Figure 4g), which was the most intensive peak of $LiTi_2(PO_4)_3$ (ICDD No. 00-035-0754), could be observed for the $TiCl_4$-modified LFP. Furthermore, an EDS measurement detected the existence of Ti in the $TiCl_4$-modified LFP as shown in Figure 4h; the Cl peak should be related to some side products from reaction between $TiCl_4$ and LFP.

Electrochemical performance.—To investigate the cyclic stability, the galvanostatic charge-discharge cycling tests were performed at 2C and 5C rates between 2.5 V and 4.2 V at room temperature. Al_2O_3 ALD-coated LFP was also tested for comparison, since Al_2O_3 film is one of the most widely used ALD coating materials in LIB but seldom used for LFP. Different thicknesses of Al_2O_3 films were coated on the LFP particles with 2, 5, and 10 cycles of Al_2O_3 ALD. In Figure S5, the 5c-Al_2O_3 delivered the same capacity as that of the UC; in Figure S6, we found that 5c-Al_2O_3 showed the best performance after 300 cycles of charge-discharge at a 2C rate, but the difference between UC and 5c-Al_2O_3 was very small. The 5c-Al_2O_3 sample was used for the following comparison studies.

We performed a long-term cycling test at a 2C rate until 1,000 cycles. In Figure 5a, the capacity of UC began to fade after 300 cycles, and 5c-Al_2O_3 began to fade after about 400 cycles. Al_2O_3 ALD coating only provide limited improvement, for one reason that Al_2O_3 and LFP are both electrically insulating materials. On the other hand, Al_2O_3 was expected to hinder the attack of HF and mitigate iron dissolution, but the results indicated a possibility of mechanical crack of LFP after repeating insertion/extraction of Li^+. Poor contact between the active material and carbon black or current collector caused by cracking will increase the internal resistance of cathode and irreversibly decrease the specific capacity. Though Al_2O_3 ALD film still demonstrated good improvement for other electrodes,[36,37] a

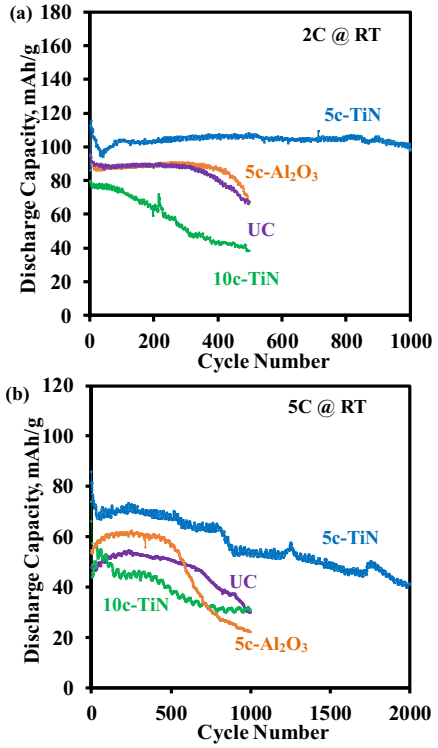

Figure 5. Cyclic performance of UC, 5c-Al_2O_3, 5c-TiN, and 10c-TiN at (a) a 2C rate for 1,000 cycles and (b) a 5C rate for 2,000 cycles between 2.5 V and 4.2 V at room temperature.

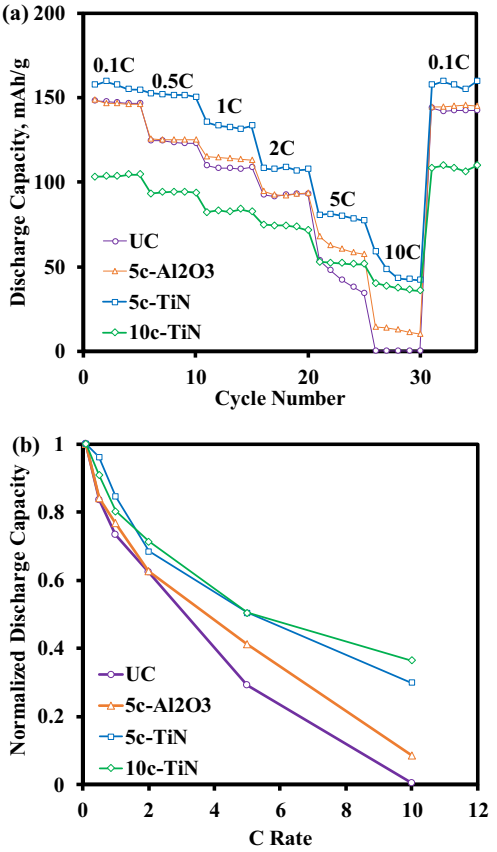

Figure 6. (a) Cyclic performance of UC, 5c-Al_2O_3, 5c-TiN, and 10c-TiN at different C rates (0.1C, 0.5C, 1C, 2C, 5C, and 10C) between 2.5 V and 4.2 V at room temperature, and (b) normalized discharge capacity of UC, 5c-Al_2O_3, 5c-TiN, and 10c-TiN at different C rates.

conductive film should be used for LFP. In contrast, 5c-TiN exhibited a stable cyclic performance even after 1,000 cycles of charge-discharge. The specific capacity of 5c-TiN was ~105 mAh/g at a 2C rate, higher than ~87 mAh/g of UC and ~88 mAh/g of 5c-Al_2O_3, which should be due to the improved conductivity by TiN ALD. The conductive TiN film would benefit the distribution of electron on the surface of LFP particles and the activity of charge transfer reaction; the Ti^{4+} dopant could improve the conductivity of LFP, stabilize the structure of LFP, and favor the Li^+ transport. However, the excessive Ti doping of 10c-TiN led to instability of cyclic performance and degradation of capacity.

A galvanostatic charge-discharge test of total 2,000 cycles at a 5C rate was also carried out. In Figure 5b, 5c-TiN showed a better capacity retention and a higher specific capacity than that of the others due to the protection of TiN film and improved conductivity by TiN films. 5c-Al_2O_3 exhibited improvement of capacity, as compared to that of UC, since the ALD film can also inhibit the growth of SPI layer and enable relaxation of strain and stress during the charge-discharge cycling.

The rate capability was investigated by galvanostatic charge-discharge cycling tests at different C rates (0.1C, 0.5C, 1C, 2C, 5C, and 10C). As shown in Figure 6a, the UC and 5c-Al_2O_3 exhibited a similar electrochemical performance, and the specific capacity at a 0.1C rate was ~149 mAh/g. Due to the existence of Al_2O_3 coating, the capacities of the 5c-Al_2O_3 at 5C and 10C exhibited a limited increase. 10c-TiN delivered a much lower capacity than the others though, as shown in Figure 6b, the 10c-TiN displayed a good rate capability at a higher current density, indicating the conductivity of 10c-TiN should be higher than that of UC, but there would be a capacity loss when Ti was over doped. On the contrary, 5c-TiN exhibited an improvement in both specific capacity and rate capability compared to those of UC. The synergic effects of TiN coating and Ti doping could strengthen LFP particles mechanically and enable a better electronic distribution and facile diffusion of Li^+, which would enhance stability and activity of LFP.

Electrochemical impedance spectroscopy (EIS) was carried out on the coin cells at their fully-discharged state before and after the 1,000-cycle test at a 2C rate and room temperature. Nyquist plots of UC, 5c-Al_2O_3, 5c-TiN, and 10c-TiN are shown in Figure 7. Every plot includes one or two semicircles and a straightly inclined line, where the semicircles describe R_f or film resistance (on the left and high-frequency region), which represents interfacial film resistance, and R_{ct} or charge transfer resistance (on the right and medium-frequency region), and W_s (the straight "tail" in the low-frequency region) is attributed to mass transfer process in the bulk. The equivalent circuit in Figure 7c was used to fit the collected EIS data.[21] R_f and R_{ct} parallel with constant phase element CPE, which represents "imperfect" double-layer capacitor. The fitting results of EIS data have been shown in Table I. Before the cycling test at a 2C rate, the sums of R_f and R_{ct} of UC and 5c-Al_2O_3 were 428 Ω and 401 Ω, respectively. In contrast, for 5c-TiN and 10c-TiN, these values were only 18 Ω and 46 Ω, indicating that the TiN ALD modification significantly improved the electronic and ionic conductivity of LFP and facilitate the kinetic of electrochemical reaction. After 1,000 cycles of charge-discharge, both UC and 5c-Al_2O_3 showed a huge increase of resistance, 612 Ω and 563 Ω, respectively, especially for the surface resistance, which means that a thick SPI layer could be formed on the surface of the cathodes. However, there was only small increase of internal resistance for 5c-TiN and 10c-TiN. Therefore, the TiN coating and Ti doping played an important role to limit the growth of SPI layer. Despite the low resistance of 10c-TiN, the cyclic performance still showed an unstable behavior, indicating that the exposure time of LFP to $TiCl_4$ should be properly controlled to avoid over-doping and the loss of capacity.

SEM analysis of cathodes was carried out on cycled cathodes of UC and 5c-TiN after 1,000-cycle charge-discharge cycling tests at a

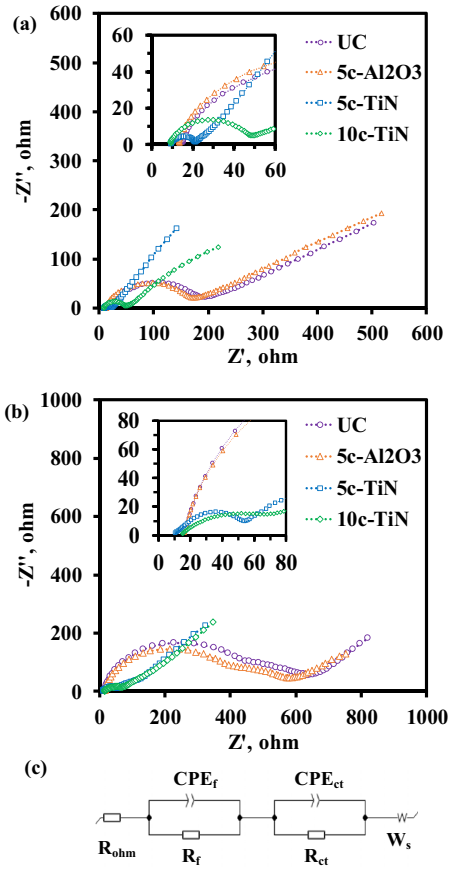

Figure 7. Nyquist plots of UC, 5c-Al_2O_3, 5c-TiN, and 10c-TiN (a) before and (b) after 1,000 cycles of charge-discharge at a 2C rate and room temperature, and (c) equivalent circuit.

2C rate and room temperature to investigate the impact of long-term cycling test at a 2C rate (Figure 8). The surfaces of cathodes were checked to compare with the SEM image shown in Figure S1. The length of time spent on SEM analysis of each sample was comparable to ensure an equal and comprehensive investigation. In Figure 8a, the surface of UC was found to be covered by a smooth and thick SPI layer, which was also observed for the overall surface of UC cathode. In contrast, there was a thinner SPI layer on cathodes from TiN modified LFP particles, as shown in Figure 8b. The modification of LFP particles by TiN ALD hindered the formation of a thick SPI layer on the top of the cathode. In Figure 8c, some cracks of LFP could be observed at some parts that were not covered by a SPI layer. More SEM images verified the presence of SPI layer and cracks on the UC cathode, as shown in Figure S7. The cracks of UC particles should be attributed to the failure caused by mechanical strain and stress during repeated insertion/extraction of Li^+, and this could result in an increase of internal resistance and an irreversible loss of capacity.

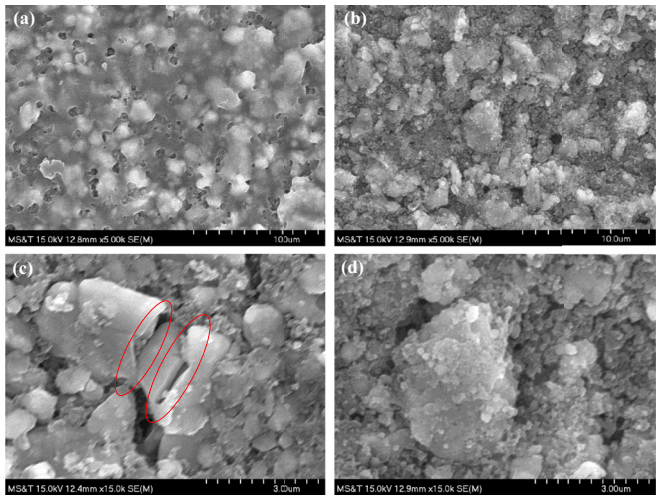

Figure 8. SEM images of (a) a thick SPI layer on the surface of UC cathode, (b) surface of 5c-TiN cathode, (c) crack on the UC particle, and (d) the well-retained particles of 5c-TiN. All SEM images of the cathodes were visualized after 1,000 charge-discharge cycles at a 2C rate and room temperature.

The 5c-TiN in Figure 8d exhibited its original shape, suggesting a good protection by TiN film and stabilization by Ti dopant, which effectively elongated the cycle life of LFP; the rough surface of active material (compared with the pristine one in Figure S1) also indicated a less influence of SPI layer on the cathode of 5c-TiN. SEM images of the surface of other parts of 5c-TiN are shown in Figure S7.

Conclusions

In this study, an effort was made to protect both surface and host structure of cathode particles and enhance kinetic of electrochemical reactions, thereby enabling higher capacity and longer cycle life. A conductive ultra-thin TiN coating was used to modify the surface of LFP particles by ALD. Due to the reaction between LFP and ALD precursor $TiCl_4$ at 400°C, Ti cation was also doped into LFP during ALD process. This modification significantly improved the conductivity and stability of LFP. During the electrochemical tests, the 5c-TiN sample achieved 93% of theoretical capacity of LFP, and the cyclic stability of 5c-TiN showed a capacity retention of ~89% after 1,000 cycles of charge-discharge at a 2C rate at room temperature, whereas the failure of uncoated LFP began after only 500 cycles. Impedance measurement and SEM images after cycling test confirmed that the synergic effects of TiN coating and Ti doping could lower the resistance, inhibit the growth of SPI layer, and strengthen the mechanical stability of the LFP particles. We also found that the exposure time of LFP to $TiCl_4$ should be properly controlled during the ALD coating process. The LFP exposed with excessive $TiCl_4$ vapor at high temperature was found to form a secondary Ti-incorporated phase, but with an expense of the original structure of LFP, and then the capacity provided by the original LFP structure was found to be significantly lower. In summary, this work proved that the synergy of

Table I. Fitting results for the EIS data.

Samples	cycle no.	R_{ohm}/ohm	R_f/ohm	R_{ct}/ohm	W_s/(ohm. $s^{-1/2}$)
UC	0	11	164	264	39
	1,000	15	370	242	46
5c-Al_2O_3	0	12	146	255	38
	1,000	15	319	244	43
5c-TiN	0	10	11	7	28
	1,000	12	25	49	53
10c-TiN	0	9	9	37	36
	1,000	14	62	39	58

TiN coating and Ti doping can effectively enhance the electrochemical performance of LFP. Furthermore, a strategy was given to utilize the instability of electrode materials in reactive conditions for an effective modification. With proper control, the complex modification, such as synergy of coating and doping during ALD, can be achieved in one step simultaneously.

Acknowledgment

This work was supported in part by the National Science Foundation (NSF DMR 1464111 and NSF CBET 1510085) and the Energy Research and Development Center (ERDC) at Missouri University of Science and Technology. The authors thank Sai Abhishek Palaparty and Seung Hyun Lee in the Department of Chemical and Biochemical Engineering at Missouri University of Science and Technology for TGA and SEM analysis.

ORCID

Jonghyun Park https://orcid.org/0000-0003-4241-3842
Xinhua Liang https://orcid.org/0000-0001-7979-0532

References

1. V. Etacheri, R. Marom, R. Elazari, G. Salitra, and D. Aurbach, *Energy & Environmental Science*, **4**, 3243 (2011).
2. M. Armand and J. M. Tarascon, *Nature*, **451**, 652 (2008).
3. D. Deng, *Energy Science & Engineering*, **3**, 385 (2015).
4. S. M. George, *Chem Rev*, **110**, 111 (2010).
5. R. W. Johnson, A. Hultqvist, and S. F. Bent, *Materials Today*, **17**, 236 (2014).
6. Y. S. Jung, A. S. Cavanagh, L. Gedvilas, N. E. Widjonarko, I. D. Scott, S.-H. Lee, G.-H. Kim, S. M. George, and A. C. Dillon, *Advanced Energy Materials*, **2**, 1022 (2012).
7. M. Yu, W. Yuan, C. Li, J.-D. Hong, and G. Shi, *Journal of Materials Chemistry A*, **2**, 7360 (2014).
8. X. Li, J. Liu, M. N. Banis, A. Lushington, R. Li, M. Cai, and X. Sun, *Energy Environ. Sci.*, **7**, 768 (2014).
9. X. Zhang, I. Belharouak, L. Li, Y. Lei, J. W. Elam, A. Nie, X. Chen, R. S. Yassar, and R. L. Axelbaum, *Advanced Energy Materials*, **3**, 1299 (2013).
10. Z. Chen, Y. Qin, K. Amine, and Y. K. Sun, *Journal of Materials Chemistry*, **20**, 7606 (2010).
11. X. Meng, X. Q. Yang, and X. Sun, *Adv. Mater*, **24**, 3589 (2012).
12. B. Xiao, H. Liu, J. Liu, Q. Sun, B. Wang, K. Kaliyappan, Y. Zhao, M. N. Banis, Y. Liu, R. Li, T. K. Sham, G. A. Botton, M. Cai, and X. Sun, *Adv Mater*, **29**, 1703764 (2017).
13. M. Xie, T. Hu, L. Yang, and Y. Zhou, *RSC Advances*, **6**, 63250 (2016).
14. F. Schipper, H. Bouzaglo, M. Dixit, E. M. Erickson, T. Weigel, M. Talianker, J. Grinblat, L. Burstein, M. Schmidt, J. Lampert, C. Erk, B. Markovsky, D. T. Major, and D. Aurbach, *Advanced Energy Materials*, **8**, 1701682 (2018).
15. R. L. Patel, Y. B. Jiang, A. Choudhury, and X. H. Liang, *Scientific Reports*, **6**, 25293 (2016).
16. M. S. Balogun, C. Li, Y. X. Zeng, M. H. Yu, Q. L. Wu, M. M. Wu, X. H. Lu, and Y. X. Tong, *Journal of Power Sources*, **272**, 946 (2014).
17. X. Lu, G. Wang, T. Zhai, M. Yu, S. Xie, Y. Ling, C. Liang, Y. Tong, and Y. Li, *Nano Letters*, **12**, 5376 (2012).
18. M. Liu, Y. Dong, Y. Wu, H. Feng, and J. Li, *Chemistry-A European Journal*, **19**, 14781 (2013).
19. M. Zhang, N. Garcia-Araez, A. L. Hector, and J. R. Owen, *Journal of Materials Chemistry A*, **5**, 2251 (2017).
20. X. H. Liang, L. F. Hakim, G. D. Zhan, J. A. McCormick, S. M. George, A. W. Weimer, J. A. Spencer, K. J. Buechler, J. Blackson, C. J. Wood, and J. R. Dorgan, *Journal of the American Ceramic Society*, **90**, 57 (2007).
21. Y. Gao, R. L. Patel, K.-Y. Shen, X. F. Wang, R. L. Axelbaum, and X. H. Liang, *ACS Omega*, **3**, 906 (2018).
22. S. Hamelet, P. Gibot, M. Casas-Cabanas, D. Bonnin, C. P. Grey, J. Cabana, J.-B. Leriche, J. Rodriguez-Carvajal, M. Courty, S. Levasseur, P. Carlach, M. Van Thournout, J.-M. Tarascon, and C. Masquelier, *Journal of Materials Chemistry*, **19**, 3979 (2009).
23. Y. Yin, M. Gao, H. Pan, L. Shen, X. Ye, Y. Liu, P. S. Fedkiw, and X. Zhang, *Journal of Power Sources*, **199**, 256 (2012).
24. C. H. Ahn, S. G. Cho, H. J. Lee, K. H. Park, and S. H. Jeong, *Metals and Materials International*, **7**, 621 (2001).
25. K.-E. Elers, J. Winkler, K. Weeks, and S. Marcus, *J Electrochem Soc*, **152**, G589 (2005).
26. J. B. Goodenough and Y. Kim, *Chemistry of Materials*, **22**, 587 (2010).
27. M. Zukalova, J. Prochazka, Z. Bastl, J. Duchoslav, L. Rubacek, D. Havlicek, and L. Kavan, *Chemistry of Materials*, **22**, 4045 (2010).
28. M. Drygaś, C. Czosnek, R. T. Paine, and J. F. Janik, *Chemistry of Materials*, **18**, 3122 (2006).
29. H. Tiznado and F. Zaera, *Journal of Physical Chemistry B*, **110**, 13491 (2006).
30. J. L. Dodd, R. Yazami, and B. Fultz, *Electrochemical and Solid-State Letters*, **9**, A151 (2006).
31. G. Y. Chen, X. Y. Song, and T. J. Richardson, *Electrochemical and Solid-State Letters*, **9**, A295 (2006).
32. L. Laffont, C. Delacourt, P. Gibot, M. Y. Wu, P. Kooyman, C. Masquelier, and J. M. Tarascon, *Chemistry of Materials*, **18**, 5520 (2006).
33. G. M. Koenig, J. W. Ma, B. Key, J. Fink, K. B. Low, R. Shahbazian-Yassar, and I. Belharouak, *J Phys Chem C*, **117**, 21132 (2013).
34. S. Patoux and C. Masquelier, *Chemistry of Materials*, **14**, 5057 (2002).
35. Z. H. Wang, Q. Q. Pang, K. J. Deng, L. X. Yuan, F. Huang, Y. L. Peng, and Y. H. Huang, *Electrochimica Acta*, **78**, 576 (2012).
36. H. Kou, X. Li, H. Shan, L. Fan, B. Yan, and D. Li, *Journal of Materials Chemistry A*, **5**, 17881 (2017).
37. H. Sopha, G. D. Salian, R. Zazpe, J. Prikryl, L. Hromadko, T. Djenizian, and J. M. Macak, *ACS Omega*, **2**, 2749 (2017).